Author's response to reviewers: Ref: SE-2019-55

Title: "Uncertainty in fault seal parameters: implications for CO_2 column height retention and storage capacity in geological CO_2 storage projects"

Our manuscript has benefited from two reviewers, Graham Yielding (R1) and Katriona Edlmann (R2). In the following we refer to the manuscript that was submitted for review as the "original manuscript", while the edited version which incorporates the reviewers comments is referred to as the "revised manuscript".
In the following the reviewer's comments are in *italic Arial* while our responses are in Times New Roman.

Author Comments to Reviewers for the open discussion.

To R1:

Dear Graham Yielding,

We are grateful for your detailed review of our manuscript. The constructive suggestions and industry insights have been very helpful and have improved and strengthened the revised manuscript. In response to the reviews received we have made a number of changes which are outlined in the "response to reviewers" which has been uploaded as supplementary information along with the revised manuscript. We hope that the revisions sufficiently address the points raised.

Kind regards,

Johannes Miocic

To R2:

Dear Katriona Edlmann,

We are grateful for your review of our manuscript. The constructive suggestions have been very helpful and have improved and strengthened the revised manuscript. In response to the reviews received we have made a number of changes which are outlined in the "response to reviewers" which has been uploaded as supplementary information along with the revised manuscript. We hope that the revisions sufficiently address the points raised.

Kind regards,

Johannes Miocic

R1

In a number of places, starting at the top of p.4, the units of IFT are incorrectly stated as mN/cm instead of mN/m - the values quoted make it clear they should all be mN/m. This should be corrected throughout the ms.

This has been adjusted in the revised manuscript.

Also at the top of page 4, I do not recognise the stated depth variability for hydrocarbon IFT. Firstly, IFT is not "fairly constant" but varies with depth. Oil IFT is stated to decrease with depth but in my experience it increases with depth - see Figure 9 of Yielding et al 2010, uploaded - from 25 mN/m at the surface to about 40 mN/m at around 3km. For methane, IFT decreases from around 75 mN/m at the surface, also to around 40 mN/m at 3km (see same figure).

We thank the reviewer for their comment. In the original submission the depth variability of hydrocarbon IFT was based on data from Schowalter (1979) and Watts (1987) and, as in the literature recommended by the reviewer, the IFT data in these publications does change with depth. The "fairly constant" statement of the original publication was supposed to illustrate that the IFT values for hydrocarbons are fairly constant at reservoir depths (1000-2000 m depth) when compared to CO_2 at these depths. However, we realise that this statement is misleading and have changed the section in the revised manuscript as follows:

"For HCs the wettability parameters IFT and θ vary with depth, particularly large changes occur between surface and conditions found at depths of 1000 m. IFT of oil increases from around 25 mN/m at very shallow conditions to around 40mN/m for conditions commonly found in reservoirs at 2.5 km depth (Yielding et al., 2010). For methane IFT is around 70 mN/m at surface conditions and decreases to 40 mN/m at subsurface conditions (Firoozabadi and Ramey, 1988; Watts, 1987). The contact angle for HCs is commonly reported as 0°(Vavra et al., 1992), simplifying equation 2 as the cosine of 0° is 1. However, for other fluids such as CO_2 the wettability parameters IFT and θ are even more pressure and temperature dependent."

On Figure 3, it is not clear to me how the CO2 lines have been derived for the two 'empirical' equations (Bretan & Yielding). I can see that the oil and methane lines differ appropriately because of their different density contrast with water. On density difference alone however, the CO2 line should be between oil and

gas, so I assume the CO2 line is reduced because of either IFT or CA input or both (in a manner similar to eqn 10). However, both the Bretan & Yielding equations were based on agglomerated oil AND gas data (i.e. the data pool is blind to fluid type), so it is not clear to me what generic 'hydrocarbon' values for IFT & CA have been assumed, in order to compute the CO2 values via eqn 10. I request that these hydrocarbon IFT and CA values be added to the caption (already contains the CO2 values).

The reviewer is correct in pointing this out. We have added the IFT and CA values to the figure caption. Additionally, we have changed the assumed IFT values for both oil and methane in the calculation of the column heights to be in line with the values suggested by the reviewer in the previous comment (IFT for methane of 60 mN/m and 30 mN/m for oil). Note that for the resulting column heights the difference between methane and CO_2 columns is even larger.

Related to the above point, the model results in D & G of Figs 5 & 6 report the effect of different ranges of wettability when using the Bretan & Yielding eqns. However, as you mention in the Discussion, these equations were derived as the maximum of observed data in oil & gas systems - so arguably they correspond to one extreme of the wettability range for hydrocarbons (least wettable). Depending on how that 'least wettable' state relates to your average CO2 wettability, I'm not sure if you are right to look at an uncertainty range which is symmetric about your chosen mean for CO2. Maybe I'm over-thinking this, perhaps you can offer a simple clarification.

We thank the reviewer for their comment. Indeed, when using the Bretan and Yielding equations the resulting column heights represent the maximum column heights instead of the average column heights resulting from the Sperrevik equations. Thus, where the Bretan and Yielding equations are used (Fig. 5&6 D&G) to analyse the influence of wettability uncertainty on column heights, we model around the least wettable state. Due to a lack of wettability data we use a normal distribution around this "least wettable" state. A more skewed distribution may better reflect the range in potential wettabilites, but this is not what we have considered here. We have clarified this in the revised manuscript by adding the following:

"Note that equations 5 to 7 result in maximum column heights (or minimal wettability) while equations 8-9 give an average column height."

And

"IFTs of 38 mN/m and 34 mN/m, and CAs of 50° and 70° are used as mean wettability for the MCMO models of reservoir A and reservoir B, respectively, based on the IFT-depth and CA-depth relationships of Iglauer (2018). For models where the approaches by Bretan et al (2003) and Yielding (2010) are used, these correspond to the mean least wettability."

The comments by the reviewer offer some intriguing ideas about how future models could be developed by using the whole input data of individual sealing faults from the Yielding and Bretan algorithms. These could be used to calculate the distribution of buoyancy pressures for a given SGR and then translating the buoyancy pressures to wettability (or pore throat size) distributions. If this could be combined with other geological data, possibly new fault seal algorithms could be developed.

In the MC modelling, do you assume that all input parameters are independent? Is this valid? (E.g. do IFT and CA co-vary for CO2?).

The reviewer points out an important point: theoretically IFT and CA should co-vary, with high IFT values corresponding with low CAs and the other way around. However, for the CO_2-brine-rock system the existing data in our opinion is too scattered to allow for a model in which they are dependent. We have added text to the revised manuscript to highlight this point as follows:

"The input parameters, which are all treated as independent, are derived from the published data described:…"

In the MC modelling, I don't think it is mentioned in the text (or tables) what value of pore-throat size is used. A value of 100 nm is mentioned in the caption of Figure 7 but it isn't clear if this is used for all other models. This is an important point, because in general in oil industry fault seal analysis it is believed that the increasing seal capacity with increasing phyllosilicate content is overwhelmingly due to a corresponding decrease in pore-throat size. Pore-throat size is observed directly in microscope analysis and also back-calculated from Hg-air injection tests. Thus your results in Fig.7, showing smaller column height for phyllosilicate-rich fault rock than for qtz-rich fault rock because of changing CA, might be countered by the qtz-rich fault rock having larger pore throats. Maybe include this pore-throat variation in the input parameters to the Fig.7 models?

We thank the reviewer for this comment, we have added the pore-throat size to the MC-modelling description in the revised manuscript. As suggested we have also added pore-size variations to the models 55-59 (two additional models) and these are shown in Figure 7. The new outcomes are discussed in the revised manuscript.

 # p1, line 15, should be "assess"

This has been changed accordingly in the revised manuscript.

 # p1, line 16, "As with" might be better than "In similarity to"

This has been changed accordingly in the revised manuscript.

 # p1, line 25, omit "," after storage

This has been changed accordingly in the revised manuscript.

 # p2, line 23, replace ";" by ":"

This has been changed accordingly in the revised manuscript.

 # p2, line 24, model not models

This has been changed accordingly in the revised manuscript.

 # p2, line 27, omit "potentially"

This has been changed accordingly in the revised manuscript.

 # p3, line 17, replace "lighter" by "less dense"

This has been changed accordingly in the revised manuscript.

 # p3, line 23, replace "transport" by "trapping" (transport is controlled by permeability)

This has been changed accordingly in the revised manuscript.

 # p4, line 9, replace "higher" by "greater"

This has been changed accordingly in the revised manuscript.

 # p4, line 22, replace "catalases" by "cataclasites"

This has been changed accordingly in the revised manuscript.

 # p4, line 24, insert "typically" before "> 1km"

This has been changed accordingly in the revised manuscript.

 # p4, line 26, replace "with" by "in"

This has been changed accordingly in the revised manuscript.

 # p5, line 24, insert "and" before "clay bed"

This has been changed accordingly in the revised manuscript.

 # p5, line 24, replace "do" by "does"

This has been changed accordingly in the revised manuscript.

 # p6, line 15, replace "sometimes" by "typically"

This has been changed accordingly in the revised manuscript.

 # p7, line 30 onwards... I was confused by FRC (fault rock composition) and FRCC (fault rock clay content). I think you only need one of these, make it consistent in text and tables.

This has been changed accordingly in the revised manuscript.

 # p9, line 3, insert "(see Figure 7)" after "57"

This has been changed accordingly in the revised manuscript.

 # p9, line 26, insert "(and hence smaller pore-throat radius)" after "content" (see earlier comment)

This has been changed accordingly in the revised manuscript.

 # Fig.4 - label the contours explicitly, to save the reader having to work out their values.

This has been changed accordingly in the revised manuscript.

 # Table 1, last column. I assume the heading should be a lower case sigma, for standard deviation? The upper case symbol confused me for a while.

This has been changed accordingly in the revised manuscript.

R2

In your abstract your statement of your findings around line 15 is not as clearly stated as it could be – especially with regards to your finding that fault composition is important and it may be worth moving your sentence beginning "In contrast to hydrocarbon systems higher phyllosilicate. . .". To before your sentence beginning "However, the wettability of the carbon dioxide system is highly sensitive. .." only to make your point that increasing phyllosilicate may not result in the expected increase in fault sealing for a co2 system.

We have changed the abstract in the revised manuscript accordingly to the reviewer's suggestions.

Page2 line 2 – while I agree that faults are ubiquitous in sedimentary basins, I would like to see a little more information provided on their extent, distribution, and scale, especially the impact of faults that are below seismic resolution.

We thank the reviewer for their comment and have added additional information on the impact of subseismic-resolution faults to the revised manuscript as follows:

"The scale and distribution of faults depends on the type of sedimentary basin and its geological history. In particularly faults that are below the resolution of seismic surveys cannot be avoided (Maerten et al., 2006; Le Gallo, 2016)."

Page 2 line 10 – faults can provide fault parallel flow for impermeable units as well? fig 1c if you are suggesting flow through the fracture – if you are not suggesting fault flow then you may nbeed to reword this section and figure.

The reviewer points out an important point. Indeed faults can provide fault parallel flow through fracture networks within otherwise impermeable units. We have updated the text describing this in the revised manuscript as follows: *"…(iii) faults can provide fault parallel flow through fracture networks in otherwise impermeable rocks linking separate permeable units…"*.

Additionally, we have adjusted the caption of figure 1.

Page 2 line 28 – "will accumulate underneath the flow barrier until breakthrough occurs due to the increase in pressure within the reservoir" what do you mean by breakthrough? Capillary, spill point, induced fracturing? Can you be clearer with this statement?

We have changed the statement in the revised manuscript accordingly as follows:

"The fluid will accumulate underneath the flow barrier until capillary breakthrough or, less frequently, induced fracturing occurs due to the increase in pressure within the reservoir."

Page 3 line 30 – perhaps add the word seal before "rocks."

This has been changed accordingly in the revised manuscript.

Page 4 line 6 – you slightly contradict your statements at the end of page 3 where you infer fine grained rocks have small pore as page 4 states "Due to the heterogeneous nature of rocks the size of pores within the sealing rock (fault rock or cap rock) varies"

We have changed this sentence in the revised manuscript to highlight that the pore sizes within caprocks generally only varies slightly. In the revised manuscript it reads as follows:

"Due to the heterogeneous nature of rocks the size of pores within the sealing rock (fault rock or cap rock) varies to a certain degree and thus two capillary pressures can be defined."

Page 8 line 5 – I would remind the reader that equations 5 to 9 are the three different author approaches (Bretan etc) as that is how you refer to them in the subsequent modelling discussions.

This has been changed accordingly in the revised manuscript as follows:

"Capillary threshold pressures for fault seals are calculated by using equations 5 to 9 (the algorithms by Bretan et al. (2003), Yielding (2010) and Sperrevik et al. (2002)), these are then converted to the CO_2-brine system using equation 10, and subsequently column heights are calculated assuming a pore-throat size of 100 nm (eq. 3)."

Discussion section – I would like to see a clearer statement of your findings and a more logical layout to your discussion as it is quite challenging to pick out the pertinent information rather than saying it "strongly influences" – I would like to see clearer statement of what he influence such as increasing phyllosilicate fault rocks results in one third less co2 stored - to make your findings clear from the start of this section which can then lead onto the detailed discussion of the reasons why.

We thank the reviewer for their suggestion and have reworked the discussion section in the revised manuscript.

Uncertainty in fault seal parameters: implications for CO_2 column height retention and storage capacity in geological CO_2 storage projects

Johannes M. Miocic[1], Gareth Johnson[2], Clare E. Bond[3]

[1]Institute of Earth and Environmental Sciences, University of Freiburg, Albertstr. 23b, 792104 Freiburg, Germany

[2] Department of Civil and Environmental Engineering, University of Strathclyde, James Weir Building, Glasgow, G1 1XJ, UK

[3] School of Geosciences, Department of Geology and Petroleum Geology, Meston Building, Aberdeen University, Aberdeen AB24 3UE, UK

Correspondence to: Johannes M. Miocic (johannes.miocic@geologie.uni-freiburg.de)

Abstract. Faults can act as barriers to fluid flow in sedimentary basins, hindering the migration of buoyant fluids in the subsurface, trapping them in reservoirs and facilitating the build-up of vertical fluid columns. The maximum height of these columns is reliant on the retention potential of the sealing fault with regards to the trapped fluid. Several different approaches for the calculation of maximum supported column height exist for hydrocarbon systems. Here, we translate these approaches to the trapping of carbon dioxide by faults and assess the impact of uncertainties in i) the wettability properties of the fault rock, ii) fault rock composition, and iii) reservoir depth, on retention potential. As with hydrocarbon systems, uncertainties associated with the wettability of a CO_2-brine-fault rock system for a given reservoir have less of an impact on column heights than uncertainties of fault rock composition. In contrast to hydrocarbon systems, higher phyllosilicate entrainment into the fault rock may reduce the amount of carbon dioxide that can be securely retained due a preferred CO_2 wettability of clay minerals. The wettability of the carbon dioxide system is highly sensitive to depth, with a large variation in possible column height predicted at 1000m and 2000m depth, the likely depth range for carbon storage sites. Our results show that if approaches developed for fault seal in hydrocarbon systems are translated, without modification, to carbon dioxide systems the capacity of carbon storage sites will be inaccurate, and the predicted security of storage sites erroneous.

Deleted: asses

Deleted: In similarity to

Deleted: However,

Deleted: In contrast to hydrocarbon systems higher phyllosilicate entrainment into the fault rock may reduce the amount of carbon dioxide that can be securely retained.

1 Introduction

Carbon capture and storage is one of the key technologies to mitigate the emission of anthropogenic carbon dioxide (CO_2) to the atmosphere (IPCC, 2005; Benson and Cole, 2008; Haszeldine, 2009; Aminu et al., 2017). Fault seal behaviour will impact geological CO_2 storage security as well as storage capacity calculations. For the successful widespread implementation of CCS, the long-term security of storage sites is vital and the fate of injected CO_2 needs to be understood. Faults are of major importance as potential fluid pathways for both vertical and lateral migration of fluids in the subsurface (Bjørlykke, 1993;

Deleted: ,

Sibson, 1994; Bense et al., 2013). Assessing whether a fault forms a lateral flow barrier or baffle for CO_2 is crucial to assessing the efficiency and safety of sub-surface carbon storage, as faults are ubiquitous in sedimentary basins, the most likely CO_2 storage reservoirs, and will naturally occur close to or within storage complexes. The scale and distribution of faults depends on the type of sedimentary basin and its geological history. In particularly faults that are below the resolution of seismic surveys cannot be avoided (Maerten et al., 2006; Le Gallo, 2016). Indeed, faults occur at many of the first industrial and pilot scale CO_2 storage sites located in sedimentary basins (e.g. In Salah, Algeria (Mathieson et al., 2010); Snøvhit, Norway (Chiaramonte et al., 2011); Ketzin, Germany (Martens et al., 2012); Otway, Australia (Hortle et al., 2013)).

Faults influence the flow and migration of fluids in three basic ways: (i) They can modify flow paths by juxtaposing stratigraphically distinct permeable and impermeable units against each other (Fig. 1a, Allan, 1989). (ii) The petrophysical properties of fault rocks can impede cross-fault flow between permeable units (Fig. 1b, Yielding et al., 1997; Aydin and Eyal, 2002; van der Zee and Urai, 2005) and (iii) faults can provide fault parallel flow through fracture networks in otherwise impermeable rocks linking separate permeable units (Fig. 1c, (Eichhubl et al., 2009; Dockrill and Shipton, 2010). i) assumes no (or minimal) permeability change in the fault zone, whereas ii) and iii) require permeability reduction and increase respectively. For CO_2 storage sites the latter two mechanisms are of particular interest and are considered here. It is worth noting that these permeability changes are temporal and dynamic and fault reactivation (Barton et al., 1995; Wiprut and Zoback, 2000) should be an important consideration in CO_2 storage projects.

Whether a fault is sealing or non-sealing is dependent on the structure and composition of the rock volume affected by, and the mechanics of, faulting (Caine et al., 1996; Aydin, 2000; Annunziatellis et al., 2008; Faulkner et al., 2010). Caine et al. (1996) describe fault zones in siliciclastic rocks defined by a fault slip surface and core and an associated damage zone, and considered the changes in permeability of a fault in this context. Fault damage zones and the fault cores are interpreted as having contrasting mechanical and hydraulic properties with the fault core being often rich in phyllosilicates which typically have low permeability while open fractures in the damage zone can have a substantially higher permeability than the host rock (Caine et al., 1996; Faulkner and Rutter, 2001; Guglielmi et al., 2008; Cappa, 2009). Models for fault zone characterisation have evolved and describe fault zones with single high-strain cores (Chester and Logan, 1986) and containing several cores (Faulkner et al., 2003), with cores and slip surfaces at the edge of the fault zone and in the middle. Perhaps to think of it simply; one model does not fit all and the heterogeneities in natural fault systems and rocks result in unique fault geometries and evolutions, albeit with similarities and semi-predictable processes.

When a fluid lighter than the pore-filling brine, such as hydrocarbons or CO_2, is introduced into a reservoir, it will naturally migrate upwards due to the buoyancy effect until it encounters a flow barrier such as a caprock or a fault. The fluid will accumulate underneath the flow barrier until capillary breakthrough or, less frequently, induced fracturing occurs due to the increase in pressure within the reservoir. The maximum vertical extent of the fluid underneath the seal before seal failure, often referred to as column height, is controlled by the fluid flow properties of the seal with regards to the fluid (Wiprut and Zoback, 2002). In the hydrocarbon industry, column heights are routinely calculated as they estimate the maximum amount of oil or

Deleted: between

Deleted: ;

Deleted: models

Deleted: potentially

gas that could be accumulated within a prospect (Downey, 1984). As the fluid flow properties of the seal may vary spatially, some uncertainty is associated with column heights, in particular when faults with their associated heterogeneities form reservoir-bounding seals. In the context of CO_2 storage, column heights represent the maximum amount of CO_2 that could be stored within a reservoir before migration out of the reservoir.

Evidence from outcrop studies indicate that faults play an important role for the migration of CO_2 in the subsurface. Both fault parallel migration of CO_2 in fault damage zones (Annunziatellis et al., 2008; Gilfillan et al., 2011; Kampman et al., 2012; Burnside et al., 2013; Keating et al., 2013, 2014; Frery et al., 2015; Jung et al., 2015; Skurtveit et al., 2017; Bond et al., 2017; Miocic et al., 2019) and across-fault migration has been reported (Shipton et al., 2004; Dockrill and Shipton, 2010). Studies of natural analogues for CO_2 storage sites have shown that if naturally occurring CO_2 reservoirs fail to retain column heights of CO_2 in the subsurface this is almost exclusively due to fault leakage (Miocic et al., 2016; Roberts et al., 2017).

In this contribution we review the main methods used to predict hydrocarbon column heights for fault bound reservoirs as applied to hydrocarbons. Placing these into a CO_2 context we consider the implications of the assumptions used and their applicability for CO_2 storage. Stochastic simulations are used to test the impact of CO_2 specific uncertainties on different fault seal algorithms, and how these affect the predicted CO_2 column height. The results highlight that fault seal parameters are poorly constrained for CO_2 and can significantly change the predicted CO_2 storage volume in fault-bounded reservoirs. Importantly, our results suggest that increasing amounts of phyllosilicates within the fault core, normally associated with increasing fault impermeability, may not necessarily increase the CO_2 column height within a reservoir.

2 Predicting fault seals for hydrocarbons and implications for CO_2 storage

As they are less dense than the pore-filling brine, hydrocarbons (HCs) migrate to the top of a reservoir where they accumulate underneath a seal. The buoyancy of HCs creates a pressure difference of ΔP at the seal-reservoir interface that is proportional to the hydrocarbon plume/column height (h) and the difference in mass density between brine (ρ_w) and HC (ρ_{hc}):

$$\Delta P = (\rho_w - \rho_{HC})\, g\, h \quad (1)$$

where g = gravitational constant and the density of HCs is dependent on the phase (gas or oil) and the in-situ pressure and temperature conditions.

The trapping of HCs within rocks is controlled by capillary forces: the interfacial tension (IFT) between HCs and the brine, the wettability of the rock/mineral surface (wetting or contact angle, θ) with respect to HCs, and the structure (size) of the pore system. Capillary pressure (P_C), the pressure difference that occurs at the interface of HCs and brine, is commonly expressed as:

$$P_c = P_{HC} - P_{brine} = \frac{2\,IFT \times \cos\theta}{r} \quad (2)$$

Deleted: lighter

Deleted: transport

Where P_{HC} is the pressure of the HC, P_{brine} is the pressure of the brine and r is the pore throat radius. P_c is inversely proportional to the pore throat radius and thus fine-grained rocks with small pores exhibit larger P_c and act as flow barrier to migrating HCs – leading to the accumulation of fluids underneath fine-grained seal rocks.

For HCs the wettability parameters IFT and θ vary with depth, particularly large changes occur between surface and conditions found at depths of 1000 m. IFT of oil increases from around 25 mN/m at very shallow conditions to around 40mN/m for conditions commonly found in reservoirs at 2.5 km depth (Yielding et al., 2010). For methane IFT is around 70 mN/m at surface conditions and decreases to 40 mN/m at subsurface conditions (Firoozabadi and Ramey, 1988; Watts, 1987). The contact angle for HCs is commonly reported as 0°(Vavra et al., 1992), simplifying equation 2 as the cosine of 0° is 1. However, for other fluids such as CO_2 the wettability parameters IFT and θ are even more pressure and temperature dependent.

Due to the heterogeneous nature of rocks the size of pores within the sealing rock (fault rock or cap rock) varies to a certain degree and thus two capillary pressures can be defined. Firstly, the capillary entry pressure (P_e), which controls the initial intrusion of the non-wetting fluid into the low permeability rock and is controlled by the radius of the largest pore throat that is in contact with the reservoir rock. Secondly, and of greater interest to column height calculations, the capillary threshold pressure (P_{th}) or sometimes called capillary breakthrough pressure, at which the wetting phase in the low permeability rock is displaced to an extent that the percolation threshold is exceeded and a continuous flow path of the non-wetting phase forms across the pore-network. The capillary threshold pressure is controlled by the smallest pore throat along the flow path, and thus $P_e < P_{th}$ applies. Seal failure occurs when buoyancy pressure is larger than capillary breakthrough pressure and the maximum supported column height follows from equations 1 and 2:

$$h = \frac{2\,IFT \times \cos\theta}{r} \times \frac{1}{(\rho_w - \rho_{HC}) \times g} \quad (3)$$

The ability of fault bound reservoirs to retain significant column heights thus depends on the fault rock composition which controls the pore-throat size (r) as well as the wettability parameters (IFT, θ). The composition and type of fault rocks in siliciclastic rocks is mainly influenced by (i) the composition of the wall rocks that are slipping past each other at the fault and in particular their content of fine grained phyllosilicate clay minerals, (ii) the stress conditions at the time of faulting, and (iii) the maximum temperature that occurred in the fault zone after faulting (Yielding et al., 2010).

In clay poor sequences (i.e. clean sandstones with less than 15% clay), the dominant fault rock types are disaggregation zones and cataclasites (Fisher and Knipe, 1998; Sperrevik et al., 2002). Disaggregation zones form during fault slip at low confining stress during early burial and constitute grain reorganization without grain fracturing. Thus they tend to have similar hydraulic properties as their host sandstones and do not form flow barriers (Fisher and Knipe, 2001). At deeper burial (typically ≥ 1 km) and higher confining stresses cataclastic processes are more significant and the resulting fractured grain fragments block the pore space resulting in higher P_{th} and in permeabilities on average one to two magnitudes lower than the host rock (Fisher and Knipe, 2001). Additionally, quartz cementation can further lower permeabilities in both disaggregation zones and cataclasites if they are subjected to post-deformation temperatures of >90°C, which equates to >3 km burial depths at typical geothermal gradients (Fisher et al., 2000).

Deleted: are fairly constant at subsurface reservoir
Deleted: , with
Deleted: decreasing
Deleted: cm
Deleted: 10mN/cm
Deleted: 25
Deleted: cm
Deleted: strongly
Deleted: higher
Deleted: catalases
Deleted: (>
Deleted: with

In sequences with intermediate clay content (15-40 % phyllosilicate), fault rocks are formed by a deformation-induced mixing of generally unfractured quartz grains and clay matrix. The resulting texture creates a fault rock with a texture termed clay-matrix gouge or phyllosilicate framework fault rock (Fisher and Knipe, 1998). Due to the clay content these fault rocks generally have high P_{th} and low permeabilities (Gibson, 1998).

In sequences dominated by clay or shale beds (>40% phyllosilicate), clay and shale rich smears can be formed on the fault plane (Weber et al., 1978). Such smears occur during ductile deformation at depths where the beds are not strongly consolidated and are often wedge-shaped, with the thickest smear adjacent to the source bed (Aydin and Eyal, 2002; Vrolijk et al., 2016). If faulting occurs at deeper burial depths where the beds are lithified, shale smears can be generated by abrasional rather than ductile processes. In such cases thin shale coatings of more or less constant thickness are formed along the fault plane (Lindsay et al., 1993). Gaps within the clay and shale smears can occur at any point (Childs et al., 2007), lowering the hydrocarbon sealing capacity of the fault rock significantly.

As direct information on fault rock composition is very rare for subsurface cases, several algorithms have been developed in the past decades to estimate the probable fault rock composition at each point of the fault surface (Weber et al., 1978; Fulljames et al., 1997; Lindsay et al., 1993). The widely used Shale Gouge Ratio (SGR) algorithm takes the average clay content of beds that slipped past any point (based on fault throw) (Yielding et al. (1997)):

$$\mathrm{SGR} = \frac{\sum(\text{Clay content} \times \text{bed thickness})}{\text{throw}} \times 100\% \quad (4)$$

SGR can be used as an estimate of fault rock composition, with high SGRs (>40-50%) the fault rock is assumed to be dominated by clay smears, while low SGRs (<15-20%) indicate that the fault rock is likely to be disaggregation zones or cataclasites (Yielding et al., 2010). The SGR algorithm, similar to other algorithms like the Shale Smear Factor (Lindsay et al., 1993), the Clay Smear Potential (Fulljames et al., 1997) or the Probabilistic Shale Smear Factor (Childs et al., 2007) which all use a combination of throw and clay bed distribution or thickness to predict the effects of clay smears, does not consider the detailed fault rock distribution and fault zone complexity observed on outcrops or at the centimetre, and sub-centimetre scale (Faulkner et al., 2010; Schmatz et al., 2010). It has however been successfully used during the last two decades to predict hydrocarbon fault seals in the subsurface (Manzocchi et al., 2010; Yielding, 2012).

Deleted: do

Two different approaches to link SGR and fault rock composition estimation with fault seal prediction parameters such as capillary threshold pressure have been developed over the years: (1) using known sealing faults to constrain relationships between SGR and HC column height and/or across fault pressure differences (Bretan et al., 2003; Yielding et al., 2010), and (2) measuring capillary threshold pressures and clay content of micro faults and correlating these to SGR, assuming that SGR is equivalent to the clay content of the fault rock (Sperrevik et al., 2002). The first approach has been fine-tuned with datasets

from sedimentary basins around the world, while equations linking capillary pressure and clay content in the second approach are derived from best-fit relationships of samples mainly from the North Sea:

$$P_{thB} = 10^{\left(\frac{SGR}{27} - C\right)} \ (Bretan\ et\ al., 2003) \quad (5)$$

with C = 0.5 for burial depths of less than 3 km, C= 0.25 for burial depths of 3.0-3.5 km and C=0 for burial depth greater than 3.5 km.

$$P_{thY} = 0.3 \times SGR - 6 \ (Yielding, 2012) \quad (6)$$

(for burial depth of less than 3 km) and

$$P_{thY} = 0.15 \times SGR + 1.9 \ (Yielding, 2012) \quad (7)$$

for burial depths of more than 3.5km, and

$$P_{thS} = 31.838 \times {k_f}^{-0.3848} \ (Sperrevik\ et\ al., 2002) \quad (8)$$

where P_{thS} is the Hg-air fault rock threshold pressure and k_f the fault rock permeability:

$$k_f = 80000 \exp\{-[19.4 \times SGR + 0.00403\, z_{max} + (0.0055\, z_f - 12.5)(1 - SGR)^7 \quad (9)$$

where z_{max} is the maximum burial depth and z_f is the depth at the time of faulting.

These three algorithms (Eq. 5-9) are widely applied to predict fault seals. In combination with equation 3 they can be used to calculate maximum fluid-column heights. While the Bretan et al. (2003) algorithm (Eq. 5) assumes an exponential correlation between the fault rock clay content (FRCC) and the capillary threshold pressure, Yielding's (2012) algorithm (Eq. 6 & 7) is based on the assumption of a linear correlation between these variables. The Sperrevik et al (2002) (Eq. 8 & 9) algorithm also assumes an exponential relationship, but tends to predict lower capillary threshold pressures than the Bretan et al (2003) algorithm (Fig. 3). Note that reported capillary pressures are typically measured in Hg-air-rock systems, which are often used to experimentally derive capillary pressures. In order to convert them to fluid-brine-rock systems, the following equation is used:

Deleted: sometimes

$$P_{HC-brine} = P_{Hg-air} \times \frac{IFT_{HC-brine} \times cos\,\theta_{HC-brine}}{IFT_{Hg-air} \times cos\,\theta_{Hg-air}} \quad (10)$$

Where P is capillary pressure, IFT interfacial tension and θ contact angle, indices indicate the fluid system. This equation highlights that uncertainties of the wettability parameters can strongly influence capillary breakthrough pressures derived from mercury injection experiments (Heath et al., 2012; Lahann et al., 2014; Busch and Amann-Hildenbrand, 2013). Thus, the results of the three algorithms are not necessarily directly comparable. Here we apply these equations (Eq. 5-10) to a CO_2 storage framework testing their veracity and analysing the revealed associated uncertainties.

3 Fault seal algorithms for CO_2

In contrast to the HC-brine-rock system, the wettability of the CO_2-brine-rock system is strongly controlled by temperature, pressure, and mineralogy (Iglauer et al., 2015b; Zhou et al., 2017). As a result, a fault seal that supports a certain hydrocarbon

column height may not necessarily support a similar amount of CO_2 (Naylor et al., 2011). This highlights the need to have a good understanding of the CO_2 wettability in the subsurface in order to establish the security of carbon storage sites.

The IFT of the CO_2-brine system is temperature, pressure and salinity dependent. It decreases from ~72 to 25 mN/m as pressure increases from atmospheric to 6.4 MPa, and plateaus at around 25±5 mN/m for supercritical CO_2 conditions and deionized water (Kvamme et al., 2007; Chiquet et al., 2007; Espinoza and Santamarina, 2010). High salinity levels, as often found in the brines filling deep saline formations, can increase the interfacial tension by up to 10 mN/m (Espinoza and Santamarina, 2010; Saraji et al., 2014). Additionally, CO_2 dissolved in the brine may decrease IFT (Nomeli and Riaz, 2017), as may impurities such as CH_4 or SO_2 (Ren et al., 2000; Saraji et al., 2014). Thus for conditions most likely for storage reservoirs – supercritical CO_2 at depths higher than 1200 m with saline brine (Miocic et al., 2016) - CO_2-brine IFT will be in the order of 35±5 mN/m (Fig. 4), similar to the range recently illustrated by Iglauer (2018).

The contact angle formed by the CO_2-brine interface on mineral surfaces varies strongly and is dependent on pressure and temperature conditions, mineral type, presence of organic matter, and the wetting phase (Sarmadivaleh et al., 2015; Espinoza and Santamarina, 2017). On water wet minerals, the contact angle (θ) is about 40° on amorphous silica and calcite surfaces, θ ~ 40° to 85° on mica, θ ~ 50° to 120° on coal, and θ ~ 8° to 30° on organic shale surfaces, while on oil wet amorphous silica θ ~ 85° to 95° (Chi et al., 1988; Chiquet et al., 2007; Chalbaud et al., 2009; Espinoza and Santamarina, 2010; Iglauer et al., 2015b; Arif et al., 2016; Espinoza and Santamarina, 2017; Guiltinan et al., 2017). With pressure rising from 10 to 15 MPa, θ increases up to 10° on quartz surfaces, while an increase of temperature from 50°C to 70°C at 10 MPa leads to an increase in θ of 15°(Sarmadivaleh et al., 2015). The CO_2 state also seems to influence the contact angle in oil-wet pores with $\theta_{gas} < \theta_{sc}$ (Li and Fan, 2015). Additionally, the wettability of rocks may shift towards more hydrophobic the longer it is exposed to a CO_2-brine mixture (Wang and Tokunaga, 2015). From the experimental data available for conditions most likely for storage reservoirs, θ in water-wet conditions will range from ~40° for quartz dominated rocks to ~70° for an organic mica rich rock (Fig. 4), with higher values likely for deeper reservoirs (Iglauer, 2018).

A general issue with the wettability data available is that most experiments are done on single, very pure and cleaned mineral surfaces and that data on the wettability of "real" subsurface rock-brine-CO_2 systems is very limited. Indeed, for potential caprock and reservoir rock lithologies such as dolomite, anhydrite, halite, mudrock, clays or fault rocks no data for subsurface conditions exists (Iglauer et al., 2015b). Recent developments for characterizing micro-scale variations of wettability in low permeability rocks may improve the knowledge in the future (Deglint et al., 2017). The wettability of fault rocks has to our knowledge not been studied experimentally yet but, as illustrated by the influence of mineralogy on contact angles, will depend on fault rock composition.

As a wide range of IFT and CA values seem possible at the CO_2 – seal interface at the subsurface conditions likely for carbon storage sites, the sealing potential of faults for CO_2 and the conditions under which faults will form seals to CO_2 flow is unclear.

4 Markov Chain Monte Carlo modelling of fault seals for CO_2

In order to better understand the impact of the uncertainties of interfacial tension and contact angle (wettability) and fault rock composition (FRC) described on commonly used fault seal algorithms when applied to CO_2, we run stochastic models where the input parameters follow probability distributions (i.e. have uncertainties associated). We use a Markov Chain Monte Carlo (MCMO) approach, which samples probability distributions of input parameters (Gilks et al., 1996), to statistically analyse the effect of uncertainties in wettability and fault rock clay content (based on SGR) on the amount of CO_2 that can be securely stored in a fault bound reservoir. The input parameters, which are all treated as independent, are derived from the published data described: empirical values from Iglauer (2018) and experimental from (Botto et al., 2017; Iglauer et al., 2015b; Saraji et al., 2014). These parameters follow a normal distribution described by the mean and the standard deviation (σ) as seen in table 1 and are sampled randomly 20,000 times for each model run. Capillary threshold pressures for fault seals are calculated by using equations 5 to 9 (the algorithms by Bretan et al. (2003), Yielding (2010) and Sperrevik et al. (2002)), these are then converted to the CO_2-brine system using equation 10, and subsequently column heights are calculated assuming a pore-throat size of 100 nm (eq. 3). Note that equations 5 to 7 result in maximum column heights (or minimal wettability) while equations 8-9 give an average column height. The resulting column heights also follow a probability distribution (table 2).

Two theoretical cases are modelled: Reservoir A is located at 1000 m depth with a temperature of 45°C, a pressure of 10.2 MPa, and with a resultant CO_2 density of 515 Kg/m³. Reservoir B is located at a depth of 1800 m, has a temperature of 69°C, a pressure of 18.36 MPa, and a resultant CO_2 density of 617 Kg/m³. Both reservoirs have a brine density of 1035 kg/m³, a maximum burial depth of 2000 m and a faulting depth of 1500 m. The normal distributions of the input parameters (FRC (SGR) and wettability of the fault rock (CA, IFT)) for the MCMO modelling are listed in table 1. IFTs of 38 mN/m and 34 mN/m, and CAs of 50° and 70° are used as mean wettability for the MCMO models of reservoir A and reservoir B, respectively, based on the IFT-depth and CA-depth relationships of Iglauer (2018). For models where the approaches by Bretan et al (2003) and Yielding (2010) are used, these correspond to the mean least wettability. For each of the reservoirs 27 models were run with 20,000 iterations each, nine models for each of approaches that link SGR to fault rock threshold pressure (eq. 5 to 9). Of these nine models three simulate varying uncertainties in CA and IFT of the fault rock (models Wet1 to Wet3), three have varying uncertainties in FRC (models FRC1 to FRC3), and three models calculate column heights based on uncertainties of FRC as well as fault rock wettability (models Comb1 to Comb3).

Five additional models investigate the impact FRC (and associated uncertainties) and the size of the pore-throat have on supported column heights for reservoir A, using equation 3. Models No. 55 to 57 simulate a quartz rich fault rock (95% of IFT within 38±2 mN/m, 95% of CA within 40±5°), a quartz-phyllosilicate mixture (95% of IFT within 38±2 mN/m, 95% of CA within 60±5°), and a phyllosilicate rich fault rock (95% of IFT within 35±2 mN/m, 95% of CA within 75±5°) with pore-throat sizes of 100±10 nm (95% interval). Models No. 58 and 59 adopt pore-throat sizes reported by Gibson (1998) for outcrop and core samples of fault zones: the pore-throat diameters of the quartz-phyllosilicate mixture of model No. 58 are intermediate (95% within 50±5 nm), and for the phyllosilicate rich fault rock of model No. 57 low (95% within 10±1 nm).

Deleted: clay content (FRCC
Deleted: ,
Deleted: (eq. 3).
Deleted: FRCC
Deleted: cm
Deleted: cm
Deleted: .
Deleted: FRCC
Deleted: FRCC
Deleted: Three
Deleted: different fault rock compositions
Deleted: Model
Deleted: simulates
Deleted: cm
Deleted: model No. 56
Deleted: cm
Deleted: model 57
Deleted: cm
Deleted: °).

The results of the MCMO models highlight the differences between the three approaches that link FRC to fault rock threshold pressure with the approach of Sperrevik et al. (2002) generally resulting in lower column heights the approaches of Bretan et al. (2003) and Yielding (2012) for both Reservoir A and B (Tab. 2, Figs. 5 & 6). Uncertainties in the wettability of fault rocks (CA, IFT) have less of an impact on the supported column height distributions than uncertainties in FRC.

For reservoir A, the models which are used to investigate the impact of uncertainties in wettability (Wet1-Wet3) have column heights ranging from 14.8±0.9 m to 14.6±3.6 m (after Sperrevik et al., 2002), and from 73±4 m to 72±18 m (after Bretan et al., 2003), and from 111±6 m to 110±27 m (after Yielding, 2012). Models which simulate uncertainties in FRC in the same reservoir have column heights ranging from 16±7 m, and from 74±14 m to 95±80 m, and from 111±14 m to 111±55 m, for the three different approaches respectively. Models which combine the uncertainties of fault rock wettability and FRC (Comb1-Comb3) have an even wider spread in column height distributions (Fig. 5c, f, i). For reservoir B, all models show a similar pattern to those of reservoir A (Fig. 6), however the mean supported column heights are only about 60% of those for reservoir A due to the differences in fault rock wettability parameters (Tabs. 1, 2). This illustrates that conditions in deeper reservoirs may lead to smaller column heights.

The results of models 55 to 59 (Fig. 7) illustrate the impact of both pore-throat size and FRC on the supported column height. For conditions similar to reservoir A a quartz rich fault rock with a pore-throat size of 100 nm (model 55) can support a column height of 118±13 m, while a mixture of quartz and phyllosilicates with the same pore-throat size (model 56) is likely to support 77±10 m, and a phyllosilicate rich fault rock (model 57) can support a column height of 40±8 m. For a smaller pore-throat size of 50 nm a mixture of quartz and phyllosilicates (model 58) can support a column height of 153±20 m, and a phyllosilicate rich fault rock with a pore-throat size of 10 nm can on average support a column height of 398±78 m. Note that the tails of the model distributions increases from model 55 to model 59. Based on the change in pore-throat sizes alone, the column heights of model 59 should be one order of magnitude larger than those of model 55.

5 Discussion

The results of the stochastic modelling illustrate that even small uncertainties in fault seal parameters can introduce significant variations, and spread, of the amount of CO_2 predicted to be securely stored within a fault-bound siliciclastic reservoir. In particular uncertainties in fault rock composition result in a wider range of possible column heights when compared to uncertainties of CO_2-brine-rock wettability. The outcomes also illustrate large differences between the algorithms used to calculate column heights. Additionally, phyllosilicate-rich fault rocks can support lower CO_2 column heights than quartz-rich fault rocks if a constant pore-throat radius is assumed.

The use of SGR as a proxy for fault rock composition, as in our study, is widely accepted and commonly used for hydrocarbon reservoirs (Fristad et al., 1997; Lyon et al., 2005). The algorithm linking SGR to fault zone threshold pressure/column height is a critical step in fault seal studies and our results show that different algorithms (Eq. 5-9) predict different CO_2 column heights. This is in line with other works comparing the three algorithms (Bretan, 2016) and is due to the sensitivity of the

Deleted: FRCC
Deleted: FRCC
Deleted: FRCC
Deleted: FRCC
Deleted: 57 highlight that
Deleted: composition
Deleted: fault rocks strongly influences
Deleted: 107±5
Deleted: 70±6
Deleted: only
Deleted: 36±6
Deleted: show
Deleted: rock wettability
Deleted: FRCC can strongly influence
Deleted: While the uncertainty associated with the CO_2 wettability of fault and top seal rocks has implications for the geological storage of CO_2, the uncertainty of the
Deleted: of the
Deleted: has a greater impact
Deleted: clay content

Sperrevik algorithm to the geological history (faulting depth and maximum burial). The algorithm has been developed from samples of North Sea cores from depths ranging from 2000-4500 m. The approaches by Bretan et al. (2003) and Yielding (2012) are both used to calculate the maximum threshold pressure, the approach by Sperrevik et al. (2002) gives an average threshold pressure. Thus, when used for a carbon storage capacity assessment, the column heights calculated with the algorithms of Bretan et al. (2003) and Yielding (2012) would illustrate the maximum potential storage capacity while the column heights resulting from the Sperrevik et al. (2002) algorithm would likely represent average capacities.

The high impact of SGR on column heights is predictable as SGR is a proxy for the amount of phyllosilicates that are incorporated into the fault rock and our results are in line with other work which highlight that good prediction of fault rock composition is crucial for hydrocarbon column height prediction (Fisher and Knipe, 2001; Yielding et al., 2010). When SGR is used for predicting fault seals in a hydrocarbon context higher SGR values coincide with higher contained column heights as high SGR value fault rocks have a higher phyllosilicate content (and hence smaller pore-throat radii). Our results show that for a CO_2 fluid the decrease in pore-throat size due to a higher phyllosilicate content results in lower column heights than anticipated. The fact that for constant pore-throat sizes phyllosilicate rich fault rocks can only support lower column heights than quartz-rich fault rocks (Fig. 7) highlights the difference between the wettability of the CO_2 –brine-rock system and the wettability of the HC-brine-rock system at subsurface conditions. Phyllosilicate minerals have contact angles of up to 85° while quartz has a contact angle around 40°(Espinoza and Santamarina, 2017; Iglauer et al., 2015a). Increasing the content of phyllosilicates in the fault rock (increasing FRCC and SGR) effectively increases the contact angle which directly reduces the capillary threshold pressure as the cosine of the contact angles approaches zero (Eq. 2). This indicates that an increase in phyllosilicates in the fault rock may not increase the amount CO_2 that can be retained by the fault to the same degree as for hydrocarbons. This calls into question whether algorithms such as SGR, which assume that higher phyllosilicate content in fault gouges equal higher sealing properties, can be used to effectively predict CO_2 fault seals. We suggest that introducing pore-throat sizes into fault seal algorithms may result in more reasonable column height predictions for CO_2 systems.

The results of our stochastic models also illustrate the impact of depth on the wettability of the CO_2-brine-rock system, with the deeper faulted reservoir scenario (at a depth of 1800 m) holding significantly lower column heights than the shallower reservoir (depth of 1000 m). This is in contrast to fault seals for hydrocarbons where faults can retain higher fluid columns for similar SGR values in deeper reservoirs (Yielding, 2012). The influence of pressure on the sealing capacity of fault rocks for CO_2 has direct implications for the selection of carbon storage sites, with shallow reservoirs being able to retain a higher column of CO_2 than deeper reservoirs (Fig. 8). Note that minimum CO_2 storage site depths are around 1000 m and are governed by the CO_2 state and density (Miocic et al., 2016).

Non-sealing faults are often undesired in a hydrocarbon exploration context, this is not necessarily true in the case of carbon storage sites. Here, sealing faults may actually reduce the amount of CO_2 that can be safely stored within a reservoir as the lateral migration of the CO_2 plume is hindered and pressure build-up may occur (Chiaramonte et al., 2015; Vilarrasa et al., 2017). If fault rocks that are sealing for hydrocarbons are not necessarily sealing for CO_2, as the results of our study suggest,

Deleted: . Contrastingly,

Deleted: of the fault rock may result

Deleted: as

Deleted: is very different at subsurface conditions from

faulted abandoned hydrocarbon reservoirs could form good carbon storage sites as long as no vertical migration of CO_2 along the fault occurs.

6 Conclusions

Fault seal modelling is associated with significant uncertainties, arising from the limited subsurface data, resolution of seismic data, faulting mechanics and fault zone structure, spatial and temporal variations, and overall limitations of scalability of observations. Nonetheless several models to estimate the sealing properties of faults have been developed and successfully used to predict hydrocarbon column heights. However, for fault seal modelling of CO_2 reservoirs the wettability of the CO_2–brine-rock system introduces additional uncertainties and reduces the amount of CO_2 that can be securely stored within a reservoir compared to hydrocarbons.

In this study uncertainties in fault rock composition, as well as uncertainties of how CO_2 fluid-rock wettability properties of the reservoir change with depth, have a stronger impact on CO_2 column heights than uncertainties in wettability. Importantly, a higher phyllosilicate content within the fault rock at a given pore-throat size, which is commonly assumed to increase the threshold pressure, may reduce the threshold pressure due to increased CO_2-wetting behaviour with such minerals. In particular deep reservoirs/high pressures seem to lead to lower column heights when compared to the equivalent predicted hydrocarbon column height.

To ensure CO_2 storage security an appropriate site characterisation for storage sites is critical. Faults of all scales must be identified and their seal potential modelled with a range of uncertainties, including the fault rock composition and wettability. During storage operations fault seal potential predictions could be refined by high resolution monitoring and development of databases similar to those used (Bretan et al., 2003; Yielding et al., 2010) to predicted hydrocarbon column heights. While fault seals may impact the storage capacities it should be kept in mind that lateral migration through non-sealing faults can increase storage capacity.

Code and data availability

Model code is available from the corresponding author upon request.

Author contributions

JMM and GJ designed the project with input from CEB. JMM developed the model code and performed the MCMO simulations. The manuscript was written by JMM with contributions from both GJ and CEB.

Acknowledgements

This work was partly supported by the Panacea project (European Community's Seventh Framework Programme FP7/2007-2013, Grant No. 282900).

References

Allan, U. S.: Model for hydrocarbon migration and entrapment within faulted structures, AAPG Bull., 73(7), 803–811, 1989.

Aminu, M. D., Nabavi, S. A., Rochelle, C. A. and Manovic, V.: A review of developments in carbon dioxide storage, Appl Energ, doi:10.1016/j.apenergy.2017.09.015, 2017.

Annunziatellis, A., Beaubien, S. E., Bigi, S., Ciotoli, G., Coltella, M. and Lombardi, S.: Gas migration along fault systems and through the vadose zone in the Latera caldera (central Italy): Implications for CO2 geological storage, Int. J. Greenh. Gas Con., 2(3), 353–372, doi:http://dx.doi.org/10.1016/j.ijggc.2008.02.003, 2008.

Arif, M., Al-Yaseri, A. Z., Barifcani, A., Lebedev, M. and Iglauer, S.: Impact of pressure and temperature on CO2–brine–mica contact angles and CO2–brine interfacial tension: Implications for carbon geo-sequestration, J. Colloid Interface Sci., 462, 208–215, doi:10.1016/j.jcis.2015.09.076, 2016.

Aydin, A.: Fractures, faults, and hydrocarbon entrapment, migration and flow, Mar. Pet. Geol., 17(7), 797–814, doi:10.1016/S0264-8172(00)00020-9, 2000.

Aydin, A. and Eyal, Y.: Anatomy of a Normal Fault with Shale Smear: Implications for Fault Seal, AAPG Bull., 86(8), 1367–1381, 2002.

Barton, C. A., Zoback, M. D. and Moos, D.: Fluid flow along potentially active faults in crystalline rock, Geology, 23(8), 683–686, doi:10.1130/0091-7613(1995)023<0683:FFAPAF>2.3.CO;2, 1995.

Bense, V. F., Gleeson, T., Loveless, S. E., Bour, O. and Scibek, J.: Fault zone hydrogeology, Earth-Sci. Rev, 127, 171–192, doi:10.1016/j.earscirev.2013.09.008, 2013.

Benson, S. M. and Cole, D. R.: CO2 Sequestration in Deep Sedimentary Formations, Elements, 4(5), 325–331, doi:10.2113/gselements.4.5.325, 2008.

Bjørlykke, K.: Fluid flow in sedimentary basins, Sediment. Geol., 86(1–2), 137–158, doi:10.1016/0037-0738(93)90137-T, 1993.

Bond, C. E., Kremer, Y., Johnson, G., Hicks, N., Lister, R., Jones, D. G., Haszeldine, R. S., Saunders, I., Gilfillan, S. M. V., Shipton, Z. K. and Pearce, J.: The physical characteristics of a CO2 seeping fault: The implications of fracture permeability for carbon capture and storage integrity, Int. J. Greenh. Gas Con., 61, 49–60, doi:10.1016/j.ijggc.2017.01.015, 2017.

Botto, J., Fuchs, S. J., Fouke, B. W., Clarens, A. F., Freiburg, J. T., Berger, P. M. and Werth, C. J.: Effects of Mineral Surface Properties on Supercritical CO2 Wettability in a Siliciclastic Reservoir, Energy Fuels, 31(5), 5275–5285, doi:10.1021/acs.energyfuels.6b03336, 2017.

Bretan, P.: Trap Analysis: an automated approach for deriving column height predictions in fault-bounded traps, Petrol. Geosci., 23(1), 56–69, doi:10.1144/10.44petgeo2016-022, 2016.

Bretan, P., Yielding, G. and Jones, H.: Using calibrated shale gouge ratio to estimate hydrocarbon column heights, AAPG Bull., 87(3), 397–413, doi:10.1306/08010201128, 2003.

Busch, A. and Amann-Hildenbrand, A.: Predicting capillarity of mudrocks, Mar. Pet. Geol., 45, 208–223, doi:10.1016/j.marpetgeo.2013.05.005, 2013.

Caine, J. S., Evans, J. P. and Forster, C. B.: Fault zone architecture and permeability structure, Geology, 24(11), 1025–1028, 1996.

Cappa, F.: Modelling fluid transfer and slip in a fault zone when integrating heterogeneous hydromechanical characteristics in its internal structure, Geophys. J. Int., 178(3), 1357–1362, doi:10.1111/j.1365-246X.2009.04291.x, 2009.

Chalbaud, C., Robin, M., Lombard, J.-M., Martin, F., Egermann, P. and Bertin, H.: Interfacial tension measurements and wettability evaluation for geological CO2 storage, Adv. Water Resour., 32(1), 98–109, doi:10.1016/j.advwatres.2008.10.012, 2009.

Chester, F. M. and Logan, J. M.: Implications for mechanical properties of brittle faults from observations of the Punchbowl fault zone, California, PAGEOPH, 124(1–2), 79–106, doi:10.1007/BF00875720, 1986.

Chi, S. M., Morsi, B. I., Klinzing, G. E. and Chiang, S. H.: Study of interfacial properties in the liquid carbon dioxide-water-coal system, Energy Fuels, 2(2), 141–145, doi:10.1021/ef00008a007, 1988.

Chiaramonte, L., White, J. A. and Trainor-Guitton, W.: Probabilistic geomechanical analysis of compartmentalization at the Snøhvit CO2 sequestration project, J. Geophys. Res. Solid Earth, 120(2), 2014JB011376, doi:10.1002/2014JB011376, 2015.

Childs, C., Walsh, J. J., Manzocchi, T., Strand, J., Nicol, A., Tomasso, M., Schöpfer, M. P. J. and Aplin, A. C.: Definition of a fault permeability predictor from outcrop studies of a faulted turbidite sequence, Taranaki, New Zealand, Geol. Soc., London, Spec. Pubs., 292(1), 235–258, doi:10.1144/SP292.14, 2007.

Chiquet, P., Daridon, J.-L., Broseta, D. and Thibeau, S.: CO2/water interfacial tensions under pressure and temperature conditions of CO2 geological storage, Energ. Convers. Manage., 48(3), 736–744, doi:10.1016/j.enconman.2006.09.011, 2007.

Deglint, H. J., Clarkson, C. R., DeBuhr, C. and Ghanizadeh, A.: Live Imaging of Micro-Wettability Experiments Performed for Low-Permeability Oil Reservoirs, Sci. Rep., 7(1), 4347, doi:10.1038/s41598-017-04239-x, 2017.

Dockrill, B. and Shipton, Z. K.: Structural controls on leakage from a natural CO2 geologic storage site: Central Utah, U.S.A., J. Struct. Geol., 32(11), 1768–1782, doi:10.1016/j.jsg.2010.01.007, 2010.

Dong, T., Harris, N. B., Ayranci, K., Twemlow, C. E. and Nassichuk, B. R.: The impact of composition on pore throat size and permeability in high maturity shales: Middle and Upper Devonian Horn River Group, northeastern British Columbia, Canada, Mar. Pet. Geol., 81, 220–236, doi:10.1016/j.marpetgeo.2017.01.011, 2017.

Downey, M. W.: Evaluating seals for hydrocarbon accumulations, AAPG Bull., 68(11), 1752–1763, 1984.

Eichhubl, P., Davatz, N. C. and Becker, S. P.: Structural and diagenetic control of fluid migration and cementation along the Moab fault, Utah, AAPG Bull., 93(5), 653–681, doi:10.1306/02180908080, 2009.

Espinoza, D. N. and Santamarina, J. C.: Water-CO2-mineral systems: Interfacial tension, contact angle, and diffusion—Implications to CO2 geological storage, Water Resour. Res., 46(7), W07537, doi:10.1029/2009WR008634, 2010.

Espinoza, D. N. and Santamarina, J. C.: CO2 breakthrough—Caprock sealing efficiency and integrity for carbon geological storage, Int. J. Greenh. Gas Con., 66(Supplement C), 218–229, doi:10.1016/j.ijggc.2017.09.019, 2017.

Faulkner, D. ., Lewis, A. . and Rutter, E. .: On the internal structure and mechanics of large strike-slip fault zones: field observations of the Carboneras fault in southeastern Spain, Tectonophysics, 367(3–4), 235–251, doi:10.1016/S0040-1951(03)00134-3, 2003.

Faulkner, D. R. and Rutter, E. H.: Can the maintenance of overpressured fluids in large strike-slip fault zones explain their apparent weakness?, Geology, 29(6), 503–506, doi:10.1130/0091-7613(2001)029<0503:CTMOOF>2.0.CO;2, 2001.

Faulkner, D. R., Jackson, C. A. L., Lunn, R. J., Schlische, R. W., Shipton, Z. K., Wibberley, C. A. J. and Withjack, M. O.: A review of recent developments concerning the structure, mechanics and fluid flow properties of fault zones, J. Struct. Geol., 32(11), 1557–1575, doi:10.1016/j.jsg.2010.06.009, 2010.

Fisher, Q. J. and Knipe, R. J.: Fault sealing processes in siliciclastic sediments, Geol. Soc., London, Spec. Pubs., 147(1), 117–134, doi:10.1144/GSL.SP.1998.147.01.08, 1998.

Fisher, Q. J. and Knipe, R. J.: The permeability of faults within siliciclastic petroleum reservoirs of the North Sea and Norwegian Continental Shelf, Mar. Pet. Geol., 18(10), 1063–1081, doi:10.1016/S0264-8172(01)00042-3, 2001.

Fisher, Q. J., Knipe, R. J. and Worden, R. H.: Microstructures of Deformed and Non-Deformed Sandstones from the North Sea: Implications for the Origins of Quartz Cement in Sandstones, in Quartz Cementation in Sandstones, edited by R. H. Worden and S. Morad, pp. 129–146, Blackwell Publishing Ltd., 2000.

Frery, E., Gratier, J.-P., Ellouz-Zimmerman, N., Loiselet, C., Braun, J., Deschamps, P., Blamart, D., Hamelin, B. and Swennen, R.: Evolution of fault permeability during episodic fluid circulation: Evidence for the effects of fluid–rock interactions from travertine studies (Utah–USA), Tectonophysics, doi:10.1016/j.tecto.2015.03.018, 2015.

Fristad, T., Groth, A., Yielding, G. and Freeman, B.: Quantitative fault seal prediction: a case study from Oseberg Syd, in Norwegian Petroleum Society Special Publications, vol. 7, edited by P. Møller-Pedersen and A. G. Koestler, pp. 107–124, Elsevier., 1997.

Fulljames, J. R., Zijerveld, L. J. J. and Franssen, R. C. M. W.: Fault seal processes: systematic analysis of fault seals over geological and production time scales, in Norwegian Petroleum Society Special Publications, vol. Volume 7, edited by P. Møller-Pedersen and A.G. Koestler, pp. 51–59, Elsevier. [online] Available from: http://www.sciencedirect.com/science/article/pii/S0928893797800069, 1997.

Gibson, R. G.: Physical character and fluid-flow properties of sandstone-derived fault zones, Geol. Soc., London, Spec. Pubs., 127(1), 83–97, doi:10.1144/GSL.SP.1998.127.01.07, 1998.

Gilfillan, S. M. V., Wilkinson, M., Haszeldine, R. S., Shipton, Z. K., Nelson, S. T. and Poreda, R. J.: He and Ne as tracers of natural CO2 migration up a fault from a deep reservoir, Int. J. Greenh. Gas Con., 5(6), 1507–1516, doi:10.1016/j.ijggc.2011.08.008, 2011.

Gilks, W. R., Richardson, S. and Spiegelhalter, D. J., Eds.: Markov Chain Monte Carlo in Practice, 1st ed., Chapman & Hall, London., 1996.

Guglielmi, Y., Cappa, F. and Amitrano, D.: High-definition analysis of fluid-induced seismicity related to the mesoscale hydromechanical properties of a fault zone, Geophys. Res. Lett., 35(6), L06306, doi:10.1029/2007GL033087, 2008.

Guiltinan, E. J., Cardenas, M. B., Bennett, P. C., Zhang, T. and Espinoza, D. N.: The effect of organic matter and thermal maturity on the wettability of supercritical CO2 on organic shales, Int. J. Greenh. Gas Con., 65, 15–22, doi:10.1016/j.ijggc.2017.08.006, 2017.

Haszeldine, R. S.: Carbon Capture and Storage: How Green Can Black Be?, Science, 325(5948), 1647, doi:10.1126/science.1172246, 2009.

Heath, J. E., Dewers, T. A., McPherson, B. J. O. L., Nemer, M. B. and Kotula, P. G.: Pore-lining phases and capillary breakthrough pressure of mudstone caprocks: Sealing efficiency of geologic CO2 storage sites, Int. J. Greenh. Gas Con., 11, 204–220, doi:10.1016/j.ijggc.2012.08.001, 2012.

Hortle, A., Xu, J. and Dance, T.: Integrating hydrodynamic analysis of flow systems and induced-pressure decline at the Otway CO2 storage site to improve reservoir history matching, Mar. Pet. Geol., 45, 159–170, doi:10.1016/j.marpetgeo.2013.04.013, 2013.

Iglauer, S.: Optimum storage depths for structural CO2 trapping, Int. J. Greenh. Gas Con., 77, 82–87, doi:10.1016/j.ijggc.2018.07.009, 2018.

Iglauer, S., Al□Yaseri, A. Z., Rezaee, R. and Lebedev, M.: CO2 wettability of caprocks: Implications for structural storage capacity and containment security, Geophys. Res. Lett., 42(21), 9279–9284, doi:10.1002/2015GL065787, 2015a.

Iglauer, S., Pentland, C. H. and Busch, A.: CO2 wettability of seal and reservoir rocks and the implications for carbon geo-sequestration, Water Resour. Res., 51(1), 729–774, doi:10.1002/2014WR015553, 2015b.

IPCC: IPCC Special report on Carbon Dioxide Capture and Storage, Cambridge University Press, New York, USA Cambridge, UK., 2005.

Jung, N.-H., Han, W. S., Han, K. and Park, E.: Regional-scale advective, diffusive, and eruptive dynamics of CO2 and brine leakage through faults and wellbores, J. Geophys. Res. Solid Earth, 2014JB011722, doi:10.1002/2014JB011722, 2015.

Kampman, N., Burnside, N. M., Shipton, Z. K., Chapman, H. J., Nicholl, J. A., Ellam, R. M. and Bickle, M. J.: Pulses of carbon dioxide emissions from intracrustal faults following climatic warming, Nature Geosci, 5(5), 352–358, doi:10.1038/ngeo1451, 2012.

Keating, E., Newell, D., Dempsey, D. and Pawar, R.: Insights into interconnections between the shallow and deep systems from a natural CO2 reservoir near Springerville, Arizona, Int. J. Greenh. Gas Con., 25(0), 162–172, doi:10.1016/j.ijggc.2014.03.009, 2014.

Keating, E. H., Newell, D. L., Viswanathan, H., Carey, J. W., Zyvoloski, G. and Pawar, R.: CO2/Brine Transport into Shallow Aquifers along Fault Zones, Environ. Sci. Technol., 47(1), 290–297, doi:10.1021/es301495x, 2013.

Kvamme, B., Kuznetsova, T., Hebach, A., Oberhof, A. and Lunde, E.: Measurements and modelling of interfacial tension for water+carbon dioxide systems at elevated pressures, Comput. Mater. Sci., 38(3), 506–513, doi:10.1016/j.commatsci.2006.01.020, 2007.

Lahann, R., Rupp, J. and Medina, C.: An evaluation of the seal capacity and CO2 retention properties of the Eau Claire Formation (Cambrian), Environ. Geosci., 21(3), 83–106, doi:10.1306/eg.05011414003, 2014.

Li, X. and Fan, X.: Effect of CO2 phase on contact angle in oil-wet and water-wet pores, Int. J. Greenh. Gas Con., 36, 106–113, doi:10.1016/j.ijggc.2015.02.017, 2015.

Lindsay, N. G., Murphy, F. C., Walsh, J. J. and Watterson, J.: Outcrop Studies of Shale Smears on Fault Surface, in The Geological Modelling of Hydrocarbon Reservoirs and Outcrop Analogues, pp. 113–123, Blackwell Publishing Ltd. [online] Available from: http://dx.doi.org/10.1002/9781444303957.ch6, 1992.

Lyon, P. J., Boult, P. J., Hillis, R. R. and Mildren, S. D.: Sealing by Shale Gouge and Subsequent Seal Breach by Reactivation: A Case Study of the Zema Prospect, Otway Basin, in Evaluating Fault and Cap Rock Seals, vol. 2, edited by P. Boult and J. Kaldi, p. 0, American Association of Petroleum Geologists., 2005.

Manzocchi, T., Childs, C. and Walsh, J. J.: Faults and fault properties in hydrocarbon flow models, Geofluids, 10(1–2), 94–113, doi:10.1111/j.1468-8123.2010.00283.x, 2010.

Martens, S., Kempka, T., Liebscher, A., Lüth, S., Möller, F., Myrttinen, A., Norden, B., Schmidt-Hattenberger, C., Zimmer, M., Kühn, M. and Group, T. K.: Europe's longest-operating on-shore CO2 storage site at Ketzin, Germany: a progress report after three years of injection, Environ. Earth Sci., 67(2), 323–334, doi:10.1007/s12665-012-1672-5, 2012.

Mathieson, A., Midgley, J., Dodds, K., Wright, I., Ringrose, P. and Saoul, N.: CO2 sequestration monitoring and verification technologies applied at Krechba, Algeria, TLE, 29(2), 216–222, doi:10.1190/1.3304827, 2010.

Miocic, J. M., Gilfillan, S. M. V., Roberts, J. J., Edlmann, K., McDermott, C. I. and Haszeldine, R. S.: Controls on CO2 storage security in natural reservoirs and implications for CO2 storage site selection, Int. J. Greenh. Gas Con., 51, 118–125, doi:10.1016/j.ijggc.2016.05.019, 2016.

Miocic, J. M., Gilfillan, S. M. V., Frank, N., Schroeder-Ritzrau, A., Burnside, N. M. and Haszeldine, R. S.: 420,000 year assessment of fault leakage rates shows geological carbon storage is secure, Sci. Rep., 9(1), 769, doi:10.1038/s41598-018-36974-0, 2019.

Nomeli, M. A. and Riaz, A.: A data driven model for the impact of IFT and density variations on CO2 storage capacity in geologic formations, Adv. Water Resour., 107, 83–92, doi:10.1016/j.advwatres.2017.06.015, 2017.

Ren, Q.-Y., Chen, G.-J., Yan, W. and Guo, T.-M.: Interfacial Tension of (CO2 + CH4) + Water from 298 K to 373 K and Pressures up to 30 MPa, J. Chem. Eng. Data, 45(4), 610–612, doi:10.1021/je990301s, 2000.

Roberts, J. J., Wilkinson, M., Naylor, M., Shipton, Z. K., Wood, R. A. and Haszeldine, R. S.: Natural CO2 sites in Italy show the importance of overburden geopressure, fractures and faults for CO2 storage performance and risk management, Geol. Soc., London, Spec. Pubs., 458(1), 181–211, doi:10.1144/SP458.14, 2017.

Saraji, S., Piri, M. and Goual, L.: The effects of SO2 contamination, brine salinity, pressure, and temperature on dynamic contact angles and interfacial tension of supercritical CO2/brine/quartz systems, Int. J. Greenh. Gas Con., 28, 147–155, doi:10.1016/j.ijggc.2014.06.024, 2014.

Sarmadivaleh, M., Al-Yaseri, A. Z. and Iglauer, S.: Influence of temperature and pressure on quartz–water–CO2 contact angle and CO2–water interfacial tension, J. Colloid Interface Sci., 441, 59–64, doi:10.1016/j.jcis.2014.11.010, 2015.

Schmatz, J., Vrolijk, P. J. and Urai, J. L.: Clay smear in normal fault zones – The effect of multilayers and clay cementation in water-saturated model experiments, J. Struct. Geol., 32(11), 1834–1849, doi:10.1016/j.jsg.2009.12.006, 2010.

Schowalter, T. T.: Mechanics of secondary hydrocarbon migration and entrapment, AAPG Bull., 63(5), 723–760, 1979.

Shipton, Z. K., Evans, J. P., Kirschner, D., Kolesar, P. T., Williams, A. P. and Heath, J.: Analysis of CO2 leakage through 'low-permeability' faults from natural reservoirs in the Colorado Plateau, east-central Utah, Geol. Soc., London, Spec. Pubs., 233(1), 43–58, doi:10.1144/GSL.SP.2004.233.01.05, 2004.

Sibson, R. H.: Crustal stress, faulting and fluid flow, Geol. Soc., London, Spec. Pubs., 78(1), 69–84, doi:10.1144/GSL.SP.1994.078.01.07, 1994.

Skurtveit, E., Braathen, A., Larsen, E. B., Sauvin, G., Sundal, A. and Zuchuat, V.: Pressure Induced Deformation and Flow Using CO2 Field Analogues, Utah, Energy Procedia, 114(Supplement C), 3257–3266, doi:10.1016/j.egypro.2017.03.1457, 2017.

Sperrevik, S., Gillespie, P. A., Fisher, Q. J., Halvorsen, T. and Knipe, R. J.: Empirical estimation of fault rock properties, in Norwegian Petroleum Society Special Publications, vol. 11, edited by Andreas G. Koestler and Robert Hunsdale, pp. 109–125. [online] Available from: http://www.sciencedirect.com/science/article/pii/S0928893702800108, 2002.

Vavra, C. L., Kaldi, J. G. and Sneider, R. M.: Geological applications of capillary pressure; a review, AAPG Bull., 76(6), 840–850, 1992.

Vilarrasa, V., Makhnenko, R. Y. and Laloui, L.: Potential for Fault Reactivation Due to CO2 Injection in a Semi-Closed Saline Aquifer, Energy Procedia, 114(Supplement C), 3282–3290, doi:10.1016/j.egypro.2017.03.1460, 2017.

Vrolijk, P. J., Urai, J. L. and Kettermann, M.: Clay smear: Review of mechanisms and applications, J. Struct. Geol., 86, 95–152, doi:10.1016/j.jsg.2015.09.006, 2016.

Wang, S. and Tokunaga, T. K.: Capillary Pressure–Saturation Relations for Supercritical CO2 and Brine in Limestone/Dolomite Sands: Implications for Geologic Carbon Sequestration in Carbonate Reservoirs, Environ. Sci. Technol., 49(12), 7208–7217, doi:10.1021/acs.est.5b00826, 2015.

Watts, N. L.: Theoretical aspects of cap-rock and fault seals for single- and two-phase hydrocarbon columns, Mar. Pet. Geol., 4(4), 274–307, doi:10.1016/0264-8172(87)90008-0, 1987.

Weber, K. J., Mandl, G. J., Pilaar, W. F., Lehner, B. V. F. and Precious, R. G.: The Role Of Faults In Hydrocarbon Migration And Trapping In Nigerian Growth Fault Structures, in OTC-3356-MS, Offshore Technology Conference, OTC., 1978.

Wiprut, D. and Zoback, M. D.: Fault reactivation and fluid flow along a previously dormant normal fault in the northern North Sea, Geology, 28(7), 595–598, doi:10.1130/0091-7613(2000)28<595:FRAFFA>2.0.CO;2, 2000.

Wiprut, D. and Zoback, M. D.: Fault reactivation, leakage potential, and hydrocarbon column heights in the northern north sea, in Norwegian Petroleum Society Special Publications, vol. 11, edited by A. G. Koestler and R. Hunsdale, pp. 203–219, Elsevier., 2002.

Yielding, G.: Using probabilistic shale smear modelling to relate SGR predictions of column height to fault-zone heterogeneity, Petrol. Geosci., 18(1), 33–42, doi:10.1144/1354-079311-013, 2012.

Yielding, G., Freeman, B. and Needham, D. T.: Quantitative fault seal prediction, AAPG Bull., 81(6), 897–917, 1997.

Yielding, G., Bretan, P. and Freeman, B.: Fault seal calibration: a brief review, Geol. Soc., London, Spec. Pubs., 347(1), 243–255, doi:10.1144/SP347.14, 2010.

van der Zee, W. and Urai, J. L.: Processes of normal fault evolution in a siliciclastic sequence: a case study from Miri, Sarawak, Malaysia, J. Struct. Geol., 27(12), 2281–2300, doi:10.1016/j.jsg.2005.07.006, 2005.

Zhou, Y., Hatzignatiou, D. G. and Helland, J. O.: On the estimation of CO2 capillary entry pressure: Implications on geological CO2 storage, Int. J. Greenh. Gas Con., 63(Supplement C), 26–36, doi:10.1016/j.ijggc.2017.04.013, 2017.

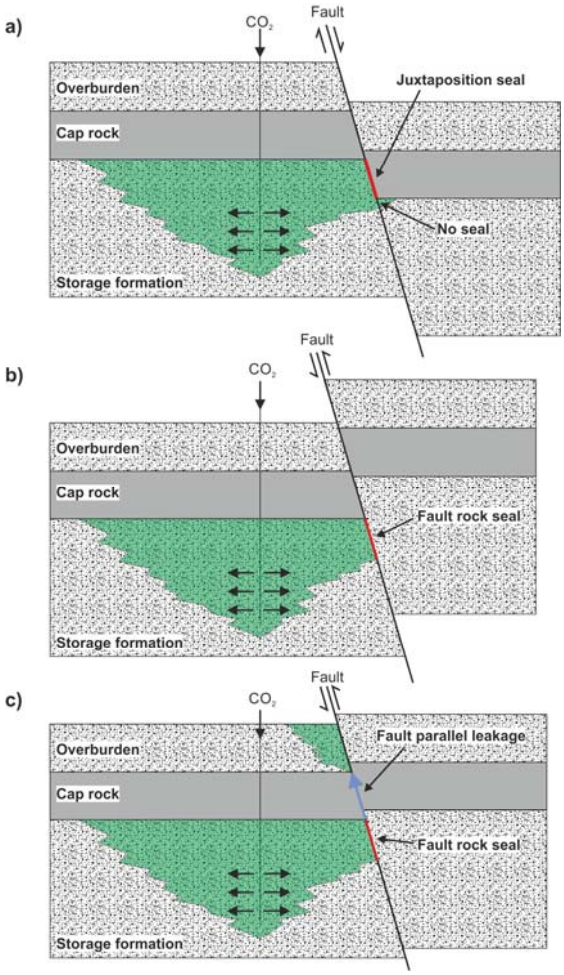

Figure 1:Impact of faults on plume migration in a CO_2 storage site. a) Juxtaposition of the permeable storage formation and impermeable cap rocks, generating a juxtaposition seal. b) Impermeable fault rocks impede fluid flow within the storage formation (fault rock seal). c) Fault parallel, vertical migration through fracture networks bypasses the cap rock.

5

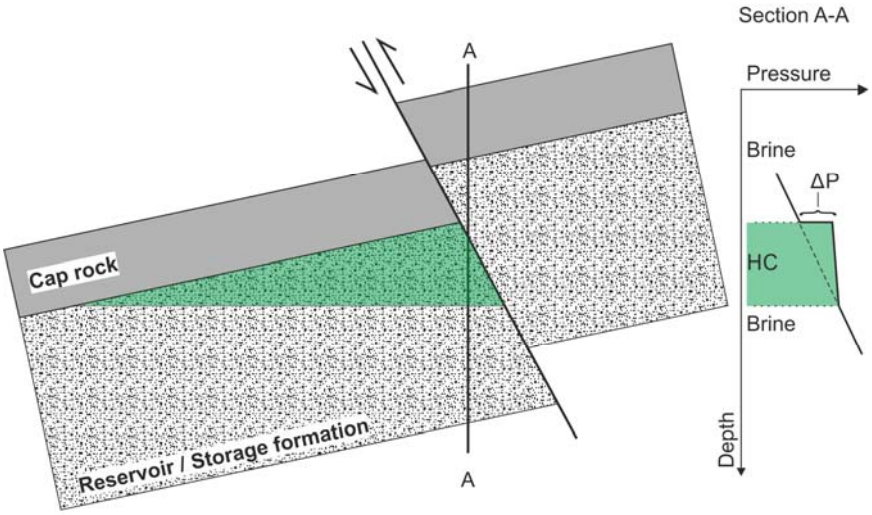

Figure 2: Injection of CO2 into a faulted geological formation where the fault is sealing. The buoyancy of CO2 creates a pressure difference at the seal and fault displayed on a pressure/depth plot for the point of the diagram labelled A-A'.

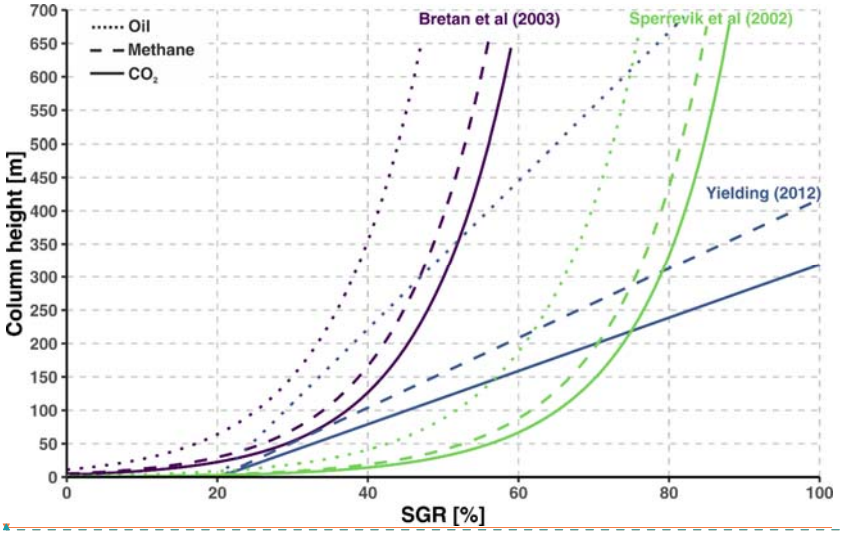

Figure 3: Plot of SGR content of fault rocks and the resulting column heights for the algorithms of Bretan et al. (2003), Sperrevik et al. (2002) and Yielding (2012) for different fluid types for a reservoir at a depth of 1000 m. Assumes contact angels of 50° for CO_2 and 0° for methane and oil, with interfacial tensions of 38 mN/m for the CO_2-brine rock system, 60 mN/m for the methane-brine-rock-system and 30 mN/m for the oil-brine-rock system. Fluid densities are 515 kg/m³ for CO_2, 75 kg/m³ for methane, 800kg/m³ for oil, and 1,035 kg/m³ for brine.

Deleted:

Formatted: Font: (Default) Arial

Deleted: a

Deleted: angle

Deleted: tension

Deleted: .

Deleted: a CO2 density of

Deleted: ³, a methane density of

Deleted: ³, an

Deleted: density of 700 kg/m³,

Deleted: a brine density of

Deleted: ³.

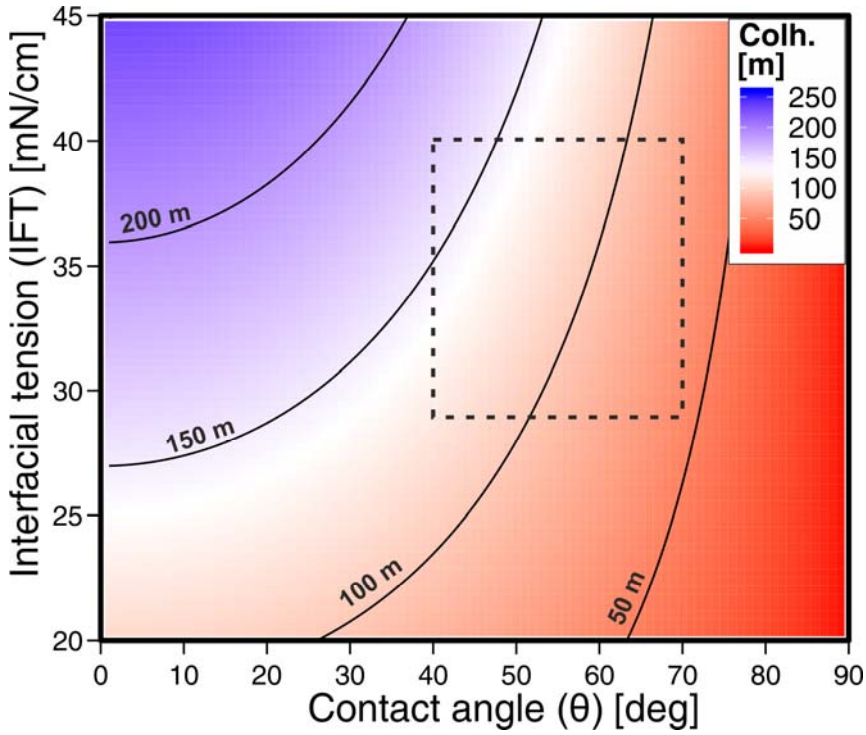

Figure 4: Figure showing the influence of contact angle (θ) and interfacial tension (IFT) on supported CO_2 column height. Black lines are contours at 50 m intervals. The full range of IFT and θ shown here has been reported for CO_2-brine-rock systems, the dashed rectangle indicates conditions likely for geological storage. Column height calculated using equations 1 and 2 with a pore throat diameter of 100 nm, a typical value for organic-poor shales (Dong et al., 2017), and a CO_2 density of 630 kg/m³, correlating to a depth of about 1500 m.

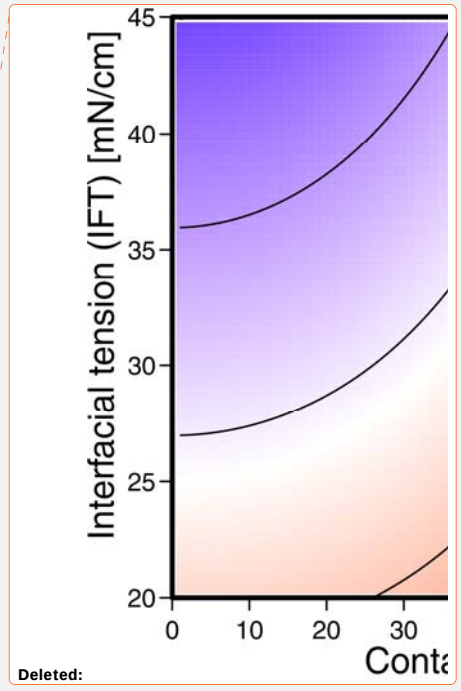

Deleted:

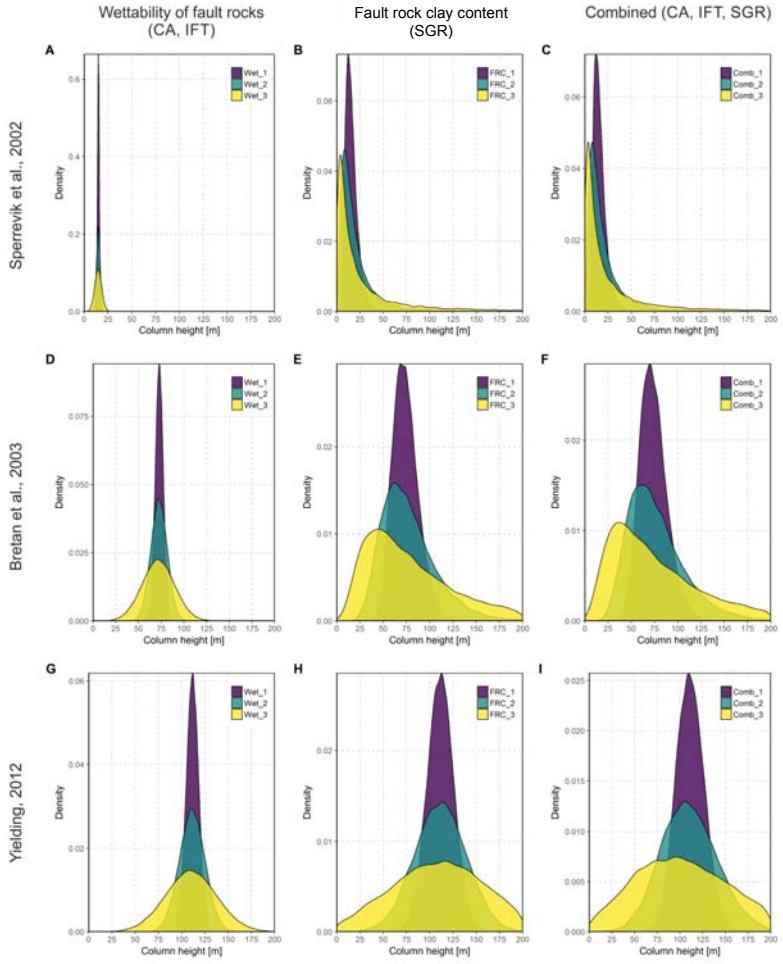

Figure 5: Density distribution of column heights of models for reservoir A (models 1 to 27). The left column (A, D, G) illustrates the impact of uncertainties in fault rock wettability, the middle column (B, E, H) the impact of uncertainties in fault rock clay content (SGR), and the right column (C,F,I) the impact of combined uncertainties on column heights. Each row uses a different approach to link fault rock composition to threshold pressure. Uncertainty increases from dark to light coloured models (Tab.1). For all models N=20.000.

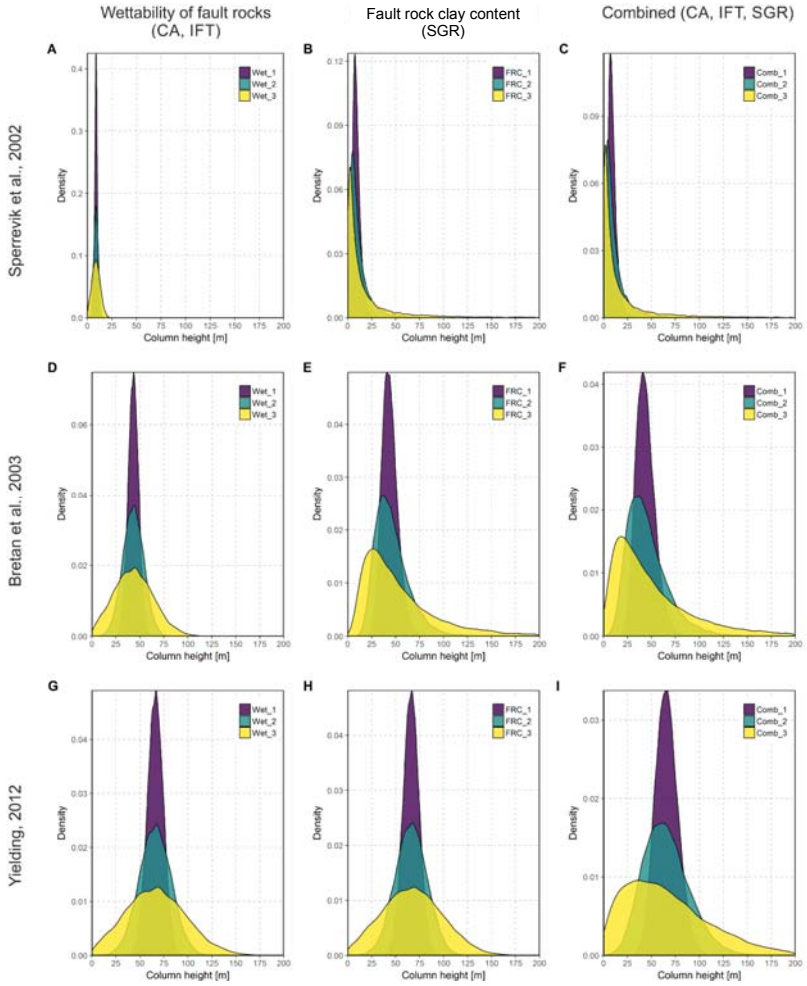

Figure 6: Density distribution of column heights of models for reservoir B (models 28 to 54). The left column (A, D, G) illustrates the impact of uncertainties in fault rock wettability, the middle column (B, E, H) the impact of uncertainties in fault rock clay content (SGR), and the right column (C,F,I) the impact of combined uncertainties on column heights. Each row uses a different approach to link fault rock composition to threshold pressure. Uncertainty increases from dark to light coloured models (Tab.1). For all models N=20.000.

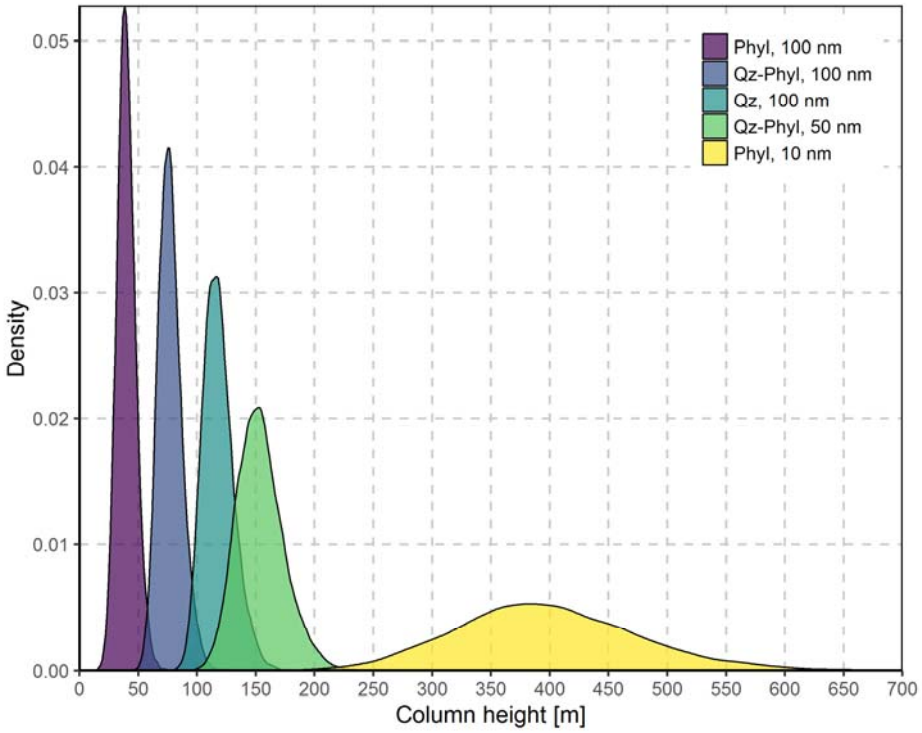

Figure 7: Density distribution of column heights of models 55 to 59 illustrates the role of fault rock composition and pore-throat size on supported column heights. If the pore-throat size is the same, phyllosilicate-rich fault rocks can only support low column heights compared to quartz rich fault rocks. If the pore-size decreases with increasing phyllosicliate content the column height increases with increasing phyllosilicate content. However, the increase in column heights is significantly less than the one order of magnitude expected due to the change in pore-throat size. This is due to the fault-rock composition depended wettability to CO_2 which results in phyllosilicate-rich fault rocks supporting a lower column than quartz rich fault rocks with a similar pore-throat. Column height is calculated using Eq. 3 and a CO_2 density of 515 kg/m³ (as Reservoir A). For all five models N=20.000.

Deleted:

Deleted: 57

Deleted: based on

Deleted: 1 and Eq.2, for a pore throat size of 100 nm,

Deleted: three

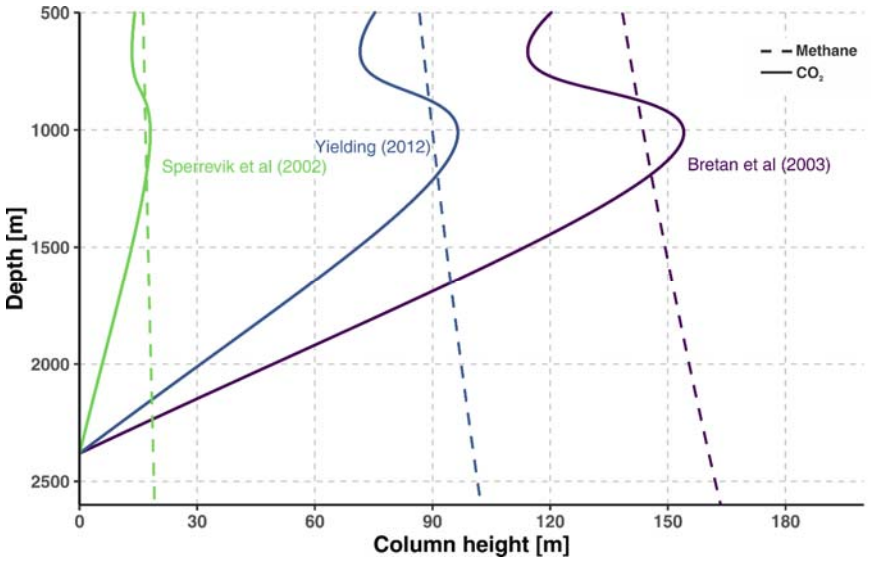

Figure 8: Supported column heights of a fault with a phyllosilicate-rich fault rock (SGR=40) depending on the depth of the fault and the trapped fluid. For CO_2 the column height decreases with depth (after an optimum at ~1000 m depth) while methane column heights increase with depth. Based on depth-wettability relationships for CO_2 by Iglauer (2018).

Table 1: Table listing the input parameters for the MCMO modelling. Reservoir A and B refer to the two theoretical reservoirs described in the text, the approach refers to the algorithm used (see text), model indicates whether uncertainties in wettability parameters (Wet), fault rock composition (FRC) or combined uncertainties (Comb) are modelled. IFT is the interfacial tension in mN/m, CA the contact angle, SGR the shale gouge ratio as parameter for fault rock composition, and PTS the pore-throat size in nm. σ is the standard deviation and describes the shape of the input normal distribution.

Model No.	Reservoir	Approach	Model	IFT	σ	CA	σ	SGR	σ
1	Reservoir A	Sperrevik et al.	Wet1	38	1	50	2.5	60	
2	Reservoir A	Sperrevik et al.	Wet2	38	2.5	50	5	60	
3	Reservoir A	Sperrevik et al.	Wet3	38	5	50	10	60	
4	Reservoir A	Sperrevik et al.	FRC1	38		50		60	5
5	Reservoir A	Sperrevik et al.	FRC2	38		50		60	10
6	Reservoir A	Sperrevik et al.	FRC3	38		50		60	20
7	Reservoir A	Sperrevik et al.	Comb1	38	1	50	2.5	60	5
8	Reservoir A	Sperrevik et al.	Comb2	38	2.5	50	5	60	10
9	Reservoir A	Sperrevik et al.	Comb3	38	5	50	10	60	20
10	Reservoir A	Bretan et al.	Wet1	38	1	50	2.5	60	
11	Reservoir A	Bretan et al.	Wet2	38	2.5	50	5	60	
12	Reservoir A	Bretan et al.	Wet3	38	5	50	10	60	
13	Reservoir A	Bretan et al.	FRC1	38		50		60	5
14	Reservoir A	Bretan et al.	FRC2	38		50		60	10
15	Reservoir A	Bretan et al.	FRC3	38		50		60	20
16	Reservoir A	Bretan et al.	Comb1	38	1	50	2.5	60	5
17	Reservoir A	Bretan et al.	Comb2	38	2.5	50	5	60	10
18	Reservoir A	Bretan et al.	Comb3	38	5	50	10	60	20
19	Reservoir A	Yielding	Wet1	38	1	50	2.5	60	
20	Reservoir A	Yielding	Wet2	38	2.5	50	5	60	
21	Reservoir A	Yielding	Wet3	38	5	50	10	60	
22	Reservoir A	Yielding	FRC1	38		50		60	5
23	Reservoir A	Yielding	FRC2	38		50		60	10
24	Reservoir A	Yielding	FRC3	38		50		60	20
25	Reservoir A	Yielding	Comb1	38	1	50	2.5	60	5
26	Reservoir A	Yielding	Comb2	38	2.5	50	5	60	10
27	Reservoir A	Yielding	Comb3	38	5	50	10	60	20
28	Reservoir B	Sperrevik et al.	Wet1	34	1	70	2.5	60	
29	Reservoir B	Sperrevik et al.	Wet2	34	2.5	70	5	60	
30	Reservoir B	Sperrevik et al.	Wet3	34	5	70	10	60	
31	Reservoir B	Sperrevik et al.	FRC1	34		70		60	5

Deleted: and

32	Reservoir B	Sperrevik et al.	FRC2	34		70		60	10
33	Reservoir B	Sperrevik et al.	FRC3	34		70		60	20
34	Reservoir B	Sperrevik et al.	Comb1	34	1	70	2.5	60	5
35	Reservoir B	Sperrevik et al.	Comb2	34	2.5	70	5	60	10
36	Reservoir B	Sperrevik et al.	Comb3	34	5	70	10	60	20
37	Reservoir B	Bretan et al.	Wet1	34	1	70	2.5	60	
38	Reservoir B	Bretan et al.	Wet2	34	2.5	70	5	60	
39	Reservoir B	Bretan et al.	Wet3	34	5	70	10	60	
40	Reservoir B	Bretan et al.	FRC1	34		70		60	5
41	Reservoir B	Bretan et al.	FRC2	34		70		60	10
42	Reservoir B	Bretan et al.	FRC3	34		70		60	20
43	Reservoir B	Bretan et al.	Comb1	34	1	70	2.5	60	5
44	Reservoir B	Bretan et al.	Comb2	34	2.5	70	5	60	10
45	Reservoir B	Bretan et al.	Comb3	34	5	70	10	60	20
46	Reservoir B	Yielding	Wet1	34	1	70	2.5	60	
47	Reservoir B	Yielding	Wet2	34	2.5	70	5	60	
48	Reservoir B	Yielding	Wet3	34	5	70	10	60	
49	Reservoir B	Yielding	FRC1	34		70		60	5
50	Reservoir B	Yielding	FRC2	34		70		60	10
51	Reservoir B	Yielding	FRC3	34		70		60	20
52	Reservoir B	Yielding	Comb1	34	1	70	2.5	60	5
53	Reservoir B	Yielding	Comb2	34	2.5	70	5	60	10
54	Reservoir B	Yielding	Comb3	34	5	70	10	60	20
Model No.	**Reservoir**		**Model**	**IFT**	**σ**	**CA**	**σ**	**PTS**	**σ**
55	Reservoir A		Qz	38	1	40	2.5	100	10
56	Reservoir A		Qz-Phy	38	1	60	2.5	100	10
57	Reservoir A		Phy	38	1	75	2.5	100	10
58	Reservoir A		Qz-Phy	38	1	60	2.5	50	5
59	Reservoir A		Phy	38	1	75	2.5	10	1

Table 2: Table showing the results of the MCMO models defined in table 1.

Model No.	**Mean column height (m)**	**Standard deviation (m)**	**2.5% per-centile (m)**	**Median column height (m)**	**97.5 % per-centile (m)**	**N**
1	14.81	0.863	13.11	14.82	16.5	20000
2	14.78	1.821	11.21	14.78	18.37	20000
3	14.62	3.629	7.536	14.61	21.81	20000

4	16.15	6.946	6.886	14.82	33.29	20000
5	22.05	28.51	3.271	14.81	83.46	20000
6	1.23E+06	1.60E+08	0.7516	14.8	1154	20000
7	16.1	7.071	6.755	14.68	33.45	20000
8	22.04	31.94	3.104	14.46	83.77	20000
9	3.38E+06	3.43E+08	0.6467	13.78	1087	20000
10	72.79	4.24	64.4	72.84	81.06	20000
11	72.61	8.945	55.08	72.61	90.24	20000
12	71.84	17.83	37.03	71.8	107.1	20000
13	73.98	13.81	50.6	72.81	104.3	20000
14	77.77	29.76	35.15	72.8	149.4	20000
15	95.2	80.8	16.97	72.77	306.6	20000
16	73.8	14.56	49.07	72.41	106.2	20000
17	77.3	31.59	32.76	71.5	154.6	20000
18	93.59	86.75	14.09	68.77	321.4	20000
19	111.5	6.494	98.62	111.5	124.1	20000
20	111.2	13.7	84.35	111.2	138.2	20000
21	110	27.31	56.7	110	164.1	20000
22	111.4	13.94	84.11	111.5	138.6	20000
23	111.3	27.88	56.7	111.5	165.6	20000
24	111.1	55.77	1.873	111.5	219.7	20000
25	111.2	15.5	81.36	110.8	142.6	20000
26	110.7	31.37	52.68	109.2	176	20000
27	109.1	63.19	1.101	103.2	247.4	20000
28	8.779	1.084	6.642	8.792	10.88	20000
29	8.761	2.2	4.468	8.769	13.11	20000
30	8.676	4.388	0.1707	8.671	17.44	20000
31	9.567	4.114	4.078	8.775	19.72	20000
32	13.06	16.88	1.938	8.772	49.43	20000
33	729600	9.45E+07	0.4452	8.765	683.7	20000
34	9.534	4.341	3.825	8.652	20.42	20000
35	13.05	19.5	1.624	8.37	51.46	20000
36	2.17E+06	2.27E+08	0.03721	7.316	641.1	20000
37	43.13	5.325	32.63	43.2	53.47	20000
38	43.05	10.81	21.95	43.09	64.41	20000
39	42.63	21.56	0.8387	42.6	85.69	20000

40	43.81	8.178	29.97	43.12	61.78	20000
41	46.06	17.63	20.82	43.12	88.49	20000
42	56.38	47.85	10.05	43.1	181.6	20000
43	43.7	9.91	27.24	42.77	65.86	20000
44	45.77	21.61	15.9	41.76	99.45	20000
45	55.43	60.6	0.5604	38.1	215.6	20000
46	66.05	8.155	49.98	66.16	81.88	20000
47	65.92	16.56	33.62	65.98	98.64	20000
48	65.28	33.02	1.284	65.24	131.2	20000
49	65.99	8.257	49.82	66.04	82.07	20000
50	65.92	16.51	33.58	66.04	98.1	20000
51	65.79	33.03	1.109	66.02	130.1	20000
52	65.84	11.71	44.45	65.38	90.08	20000
53	65.52	23.81	25.16	63.56	118	20000
54	64.57	49.28	-6.554	56.9	180.7	20000
55	117.8	13.21	95.41	116.7	147.2	20000
56	76.88	10.04	59.46	76.14	99.08	20000
57	39.76	7.8	25.69	39.32	56.45	20000
58	153.8	20.09	118.9	152.3	198.2	20000
59	397.6	78	256.9	393.2	564.5	20000